Carbohydrate Polymers 346 (2024) 122604

Contents lists available at ScienceDirect

Carbohydrate Polymers

journal homepage: www.elsevier.com/locate/carbpol

Tailoring the structural and physicochemical properties of rice straw cellulose-based cryogels by cell-mediated polyhydroxyalkanoate deposition

Laura Cabrera-Villamizar [a], Cristina Campano [b,c,*], Amparo López-Rubio [a,b], María José Fabra [a,b,*], M. Auxiliadora Prieto [b,c]

[a] Food Safety and Preservation Department, Institute of Agrochemistry and Food Technology (IATA), CSIC, Carrer del Catedràtic Agustín Escardino Benlloch, 7, 46980, Valencia, Spain
[b] Interdisciplinary Platform for Sustainable Plastics towards a Circular Economy—Spanish National Research Council (SusPlast), CSIC, Madrid 28006, Spain
[c] Polymer Biotechnology Group, Biological Research Centre Margarita Salas, Spanish National Research Council (CIB), CSIC, C. Ramiro de Maeztu, 9, 28040 Madrid, Spain

ARTICLE INFO

Keywords:
Rice straw
Cryogels
Cellulose
Polyhydroxyalkanoates
Water vapor sorption

ABSTRACT

This study presents a novel biotechnological approach for creating water vapor-resistant cryogels with improved integrity. Rice straw cellulose was transformed into nanofibrils through TEMPO-mediated oxidation and high-pressure homogenization. The resulting cryogels remained firm even when immersed in aqueous media, whose pores were used by live cell to deposit polyhydroxyalkanoate (PHA) particles inside them. This novel method allowed the compatibilization of PHA within the cellulosic fibers. As a consequence, the water sorption capacity was decreased by up to 6 times having just 4 % of PHA compared to untreated cryogels, preserving the cryogel density and elasticity. Additionally, this technique can be adapted to various bacterial strains and PHA types, allowing for further optimization. It was demonstrated that the amount and type of PHA (medium chain length and small chain length-PHA) used affects the properties for the cryogels, especially the water vapor sorption behavior and the compressive strength. Compared to traditional coating methods, this cell-mediated approach not only allows to distribute PHA on the surface of the cryogel, but also ensures polymer penetration throughout the cryogel due to bacterial self-movement. This study opens doors for creating cryogels with tunable water vapor sorption and other additional functionalities through the use of specialized PHA variants.

1. Introduction

In recent years, the development of porous materials (aerogels and cryogels) has grown rapidly due to their diverse applications, which include thermal and acoustic insulation (Do et al., 2020; Hasan et al., 2017), transport of active substances (García-González et al., 2021), moisture absorption, and flame retardancy (Farooq et al., 2018). In particular, a cryogel is a type of hydrogel that is formed by cryotropic gelation, which involves freezing a polymer suspension at low temperatures. The freezing process leads to the formation of ice crystals that act as a template for the porous structure of the cryogel. Cryogels have low density and an interconnected porous structure, which makes them suitable for various applications such as tissue engineering, drug delivery and water purification (Nayak & Das, 2018). In cryogel development, the use of biopolymers as an alternative to non-renewable materials is gaining attention. For example, several porous cellulosic materials have been developed to accomplish the same functionalities of traditional synthetic materials, while offering additional value by being biocompatible and biodegradable. Porous cellulosic materials possess advantages compared to other 3D networks, such as low density, high porosity, and large surface area, making them very promising materials for the 21st century (Long et al., 2018).

However, the inherent hydrophilicity of cellulose has sometimes limited its application as material due to its fibrillar separation in water environments, thus affecting the integrity of the 3D cellulose networks formed during cryogel formation when exposed to high humidity environments (Etale et al., 2023). Several techniques have been proposed to address this challenge, including coatings and chemical modifications

* Corresponding authors at: Interdisciplinary Platform for Sustainable Plastics towards a Circular Economy—Spanish National Research Council (SusPlast), CSIC, Madrid 28006, Spain.
E-mail addresses: la.cabrera10@iata.csic.es (L. Cabrera-Villamizar), cristina.campano@cib.csic.es (C. Campano), amparo.lopez@iata.csic.es (A. López-Rubio), mjfabra@iata.csic.es (M.J. Fabra), auxi@cib.csic.es (M.A. Prieto).

https://doi.org/10.1016/j.carbpol.2024.122604
Received 13 June 2024; Received in revised form 5 August 2024; Accepted 8 August 2024
Available online 10 August 2024

that reduce the water permeability of the material (Feng et al., 2015). One promising method involves the previous modification of cellulose pulp to produce cellulose nanofibers (CNFs) before material formulation, which can be achieved by TEMPO-mediated oxidation coupled to high-pressure homogenization (Fiol et al., 2019). The oxidation of hydroxyl groups of cellulose to carboxylic groups during TEMPO-mediated oxidation facilitates fiber separation due to repulsive charges, while subsequent high-pressure homogenization separates fibers, reduces their size, and promotes water retention within the formed network (Besbes et al., 2011). Thus, once these CNFs are subjected to a drying process, these hydrogen bonds acquired during the production process between the carboxyl groups of the CNFs and water are modified in such a way that new hydrogen bonds are formed between fibrils, increasing the anchorage points between them after drying and thus facilitating their physical integrity once submerged again into water. Our hypothesis is that TEMPO-treated cellulose homogenized at high pressure, followed by freeze-drying, would allow the fabrication of cryogels that can be subjected to further modification processes in aqueous media.

In addition, cellulose production is increasingly focusing on sustainability. The revalorization of industrial waste offers a promising approach, using waste products as raw materials. Rice straw (RS), a waste generated worldwide estimated at 780 million tons per year, is a good example of this type of biomass (Freitas et al., 2022). This biomass can be converted into cellulose and processed to produce cryogel-type materials. However, cellulosic materials are still sensitive to moisture and have a high-water vapor transmission rate. To solve this problem, cellulose-derived materials have been externally coated with various additives and coatings, such as methyltrimethoxylan (Feng et al., 2015), polylactic acid (Benito-González et al., 2020), polylactic acid/polyhydroxybutyrate (Reyes et al., 2023), polycaprolactone, cellulose acetate, poly(methyl methacrylate) (Pircher et al., 2014), among others.

In this study, polyhydroxyalkanoates (PHAs) were proposed as water-repellent agents for cellulosic cryogel materials. PHAs are biobased polyesters synthesized by microorganisms of different genera with high hydrophobic properties (Hernández-Arriaga et al., 2022). They are classified according to the length of their 3-hydroxyalkanoate (3HA) repeat units. Short-chain PHAs (scl-PHA) typically have 4–5 carbon atoms per 3HA unit, whereas medium-chain PHAs (mcl-PHA) have 6–14 carbons. This difference in chain length results in different material properties. Scl-PHAs are typically crystalline and biodegradable, with high melting points, whereas mcl-PHAs are amorphous, elastomeric and compostable, and exhibit lower melting points and degrees of crystallinity (Kourmentza et al., 2017; Reddy et al., 2022). Poly(3-hydroxybutyrate (PHB) and poly(3-hydroxyvalerate) (PHV) are examples of scl-PHA, while the example of mcl-PHA could be poly (hydroxyoctanoate-co-hydroxyhexanoate) [P(HO-co-HX] (Martínez et al., 2012). These materials exhibit versatility and can be used for specific applications; for example, scl-PHA has better barrier properties than mcl-PHA (Silva et al., 2021). In addition, various functionalities have been reported as carriers and hydrophobizing agents (Fabra et al., 2016; Urbina et al., 2019).

In a recent work, Campano et al., 2022 developed bacterial cellulose (BC)-PHA films using a methodology consisting in the colonization of BC membranes by bacteria that had previously accumulated PHA intracellularly, which was released by a mild acid treatment. Using this strategy, it was possible to produce films with better gas barrier properties than even the plastic films commonly used for this purpose. BC offers several advantages, such as its high purity and unique properties. However, its high production cost and limited availability make it difficult to apply on a large scale. Cellulose derived from agricultural residues, such as RS, presents a promising alternative due to its abundance and lower production cost. However, the different water behavior of cellulose compared to hydrophobic polymers such as PHA has limited its compatibility in the manufacture of composite materials.

This work proposes a novel strategy to develop biocompatible cryogels with controllable water vapor sorption properties. We hypothesize that by combining non-water-dispersible CNF cryogels and using PHA-producing bacteria for targeted deposition of PHA within the pores, we can achieve superior control over water vapor sorption behavior compared to traditional methods. The method combines TEMPO-mediated oxidation and high-pressure homogenization-enhanced cellulose matrix and PHA-producing bacteria. First, TEMPO-mediated oxidation combined with high-pressure homogenization was used to create cellulosic cryogels. This pretreatment strengthens the cellulose network by increasing hydrogen bonds firstly with water molecules, and then between nanofibers when cryogel is becoming dried, which may ensure that the cryogels maintain their integrity when immersed in aqueous media.

Subsequently, live bacteria will act in this study as PHA producers and carriers. These bacteria would enter the pores of the material and colonize the cellulosic network, depositing PHA granules where the cells were placed using a mild acid treatment. This biocompatible deposition offers a significant advantage over traditional methods, in which PHA usually coats the outer layer of the cryogel (Reyes et al., 2023). This combined approach is expected to yield cellulosic cryogels with several key benefits. First, TEMPO pretreatment might ensure that the cryogels remain with a stable structure in aqueous media. In addition, bacterial-driven PHA deposition would promote precise placement of PHA granules within the cryogel pores for optimal interaction and functionality. Finally, the inherent properties of both cellulose and PHAs, coupled with the controlled deposition offered by bacteria, could allow for tailoring water vapor sorption behavior to specific applications. The versatility of this method may enable further customization by strategically employing different bacterial strains and PHA types to achieve desired functionalities in various materials.

2. Materials and methods

2.1. Materials

RS was collected in September of 2021 (Sueca, Spain). The material was ground using an industrial mill with 3 mm and 1.5 mm mesh and then was stored in plastic boxes until further processing. The reagents used in this study were of analytical grade. Toluene (≥99.5 %, VWR chemicals), ethanol (96 %, Scharlab), $NaClO_2$ (80 %, Sigma-Aldrich), glacial acetic acid (≥ 99.7 %, Labkem), KOH (90 %, Sigma-Aldrich), TEMPO (98 %, Sigma-Aldrich), NaBr (≥99 %, Sigma-Aldrich), NaClO sodium hypochlorite solution (10–15 %, Sigma-Aldrich), NaCl (99 %, Panreac), NaOH (≥98 %, Panreac), Luria Bertani culture media (Labkem), Kanamycin disulfate salt (Sigma-Aldrich), IPTG (Sigma-Aldrich), Cellulase from *Trichoderma reesei* (≥700 units/g, Sigma-Aldrich), H_2SO_4 (99 %, Sigma-Aldrich), methanol (≥99.9 %, Sigma-Aldrich), chloroform (98 %, Panreac), 3-methylbenzoic acid (≥98 %, Sigma-Aldrich) and Na_2SO_4 (≥99 %, Sigma-Aldrich). For M63 0.1 N nitrogen-limited minimal medium the reagents used were: KH_2PO_4 (≥99 %, Sigma-Aldrich), $(NH_4)_2SO_4$ (≥99 %, Sigma-Aldrich), $FeSO_4 \bullet 7\ H_2O$ (≥99 %, Sigma-Aldrich), $MgSO_4$ (≥98 %, Sigma-Aldrich), $MnCl_2 \bullet 4H_2O$, $CoSO_4 \bullet 7H_2O$ (Supelco), $CaCl_2 \bullet 2H_2O$ (≥93 %, Honeywell), $CuCl_2 \bullet 2H_2O$ (≥99 %, Honeywell), $ZnSO_4 \bullet 7H_2O$ (Supelco) and sodium octanoate (96 %, Thermo Scientific).

2.2. Cellulose extraction from RS

The extraction of cellulose was carried out according to Benito-González et al., 2022. Concisely, 7 g of RS was added to cellulose extraction thimbles and placed in a multiple Soxhlet equipment (Soxtec™ 8000, FOSS Analytics) with 75 mL of toluene: ethanol in a 2:1 ratio in order to extract waxes, lipids and pigments. Extraction was performed at 210 °C with 30 min boiling, 1 h 30 min extraction and a final 10 min solvent recovery step. The samples were evaporated in a fume hood for 24 h and then dried at 60 °C. The solid fraction from this first step was referred to as fraction 1 (F1).

To obtain fraction 2 (F2), the lignin was bleached and removed by oxidative treatment. 9.8 g of $NaClO_2$ was dissolved in 700 mL of distilled water and the pH was adjusted to 3 with glacial acetic acid. The suspension was heated to 70 °C and 7 g of F1 was added. The mixture was stirred at 200 rpm for 5 h. The process was then stopped in an ice bath and the sample was filtered through a nylon cloth with a pore size of 15 μm. The material was washed with distilled water to neutral pH.

Finally, to prepare fraction 3 (F3), hemicelluloses were removed by alkali treatment. Precisely, 4 g of F2 was added to 400 mL of KOH (5 % w/v) and the suspension was stirred at room temperature for 24 h. Subsequently, the temperature was raised to 90 °C for 2 h and the sample was filtered through a nylon cloth with a pore size of 15 μm. The material was washed with distilled water to neutral pH. The partially hydrated materials were stored at 4 °C and the water content was determined in each case by applying a known mass of the gel and weighing it after 16 h at 60 °C.

The carbohydrate composition of the obtained fractions was analyzed using high performance anion exchange chromatography with pulsed amperometric detection (HPAEC-PAD, Dionex) according to (Pérez-Bassart et al., 2023). Additionally, the Klason lignin content in the fractions was determined according to the TAPPI T222 om-06 method, with slight modifications according to (Cebrián-Lloret et al., 2022).

2.3. TEMPO-mediated oxidation and high-pressure homogenization

To obtain a cellulose nano/microfiber (CNF), the protocol of Isogai et al., 2011 was used with some modifications specified below. Briefly, 1 mmol of TEMPO and 10 mmol of NaBr were dissolved in 1 L of deionized water. Once the solution was homogeneous, 10 g of F3 (dry weight of cellulose extract) was added. Next, 90 mL of 10 % NaClO (50 mmol) was added, and the pH was adjusted on demand to prevent it from falling below 10. The reaction was continued until no pH change was detected, and then the oxidized material was washed with deionized water. The partially hydrated material was stored at 4 °C and the water content was determined by applying a known mass of the gel and weighing it after 16 h at 60 °C. Subsequently, the pulp was dispersed in deionized water to obtain a 1 % (w/v) suspension. The suspension was magnetically stirred and subjected to ultrasound in an ice bath using the Sonicator 450 (BRANSON Ultrasonics Corporation, USA) under maintenance, duty cycle of 20 and output control of 3.5, for 5 min cycles until completely homogeneous. Subsequently, the nanocellulose suspension was homogenized using a GEA PandaPLUS 2000 high-pressure homogenizer (Düsseldorf, Germany) at 600 bar for 2, 4 and 8 high-pressure homogenization (HPH) passes. The suspensions were collected and stored separately after each homogenization step (after 2, 4 and 8 HPH passes). The final homogenized nanocellulose (CNF) suspensions were stored at 4 °C until further use.

Carboxyl groups obtained with the TEMPO-mediated oxidation reaction were determined by conductometric titration with 0.15 g of dry pulp. 5 mL of NaCl 0.01 M and deionized water were added to a total volume of 50 mL. Then, 0.1 M HCl were added to adjust the pH to 2.8 to protonate the carboxyl groups. NaOH 0.05 M was added in 0.1 mL increments and the conductimetry values were recorded. The carboxyl groups are determined by Eq. (1).

$$carboxyl\ groups\ \frac{mmol\ COOH}{g\ dry\ pulp} = \frac{(Ve\ (ml) - Vi\ (ml)\ )*NaOH\ molarity\ (M)}{dry\ pulp\ (g)} \quad (1)$$

Where, Vi and Ve are the volume of NaOH in the initial and the end points in which the conductivity is constant (Xu et al., 2022).

The network conformation, fiber spacing and fiber thickness were characterized by transmission electron microscopy (TEM). Sample preparation followed the method of Bandara and Wu (2018) with modifications. Briefly, 0.02 % suspensions were prepared by sonicating the sample in deionized water. Subsequently, 10 μL of the suspension was applied on copper TEM grids and allowed to dry at room temperature (22 ± 2 °C) for 2 h. Excess liquid was removed with filter paper. The dried samples were stained with 2 % uranyl acetate. TEM images were obtained with a JEOL JEM-1010 microscope (JEOL Ltd., Japan) operated at 80 kV. Fiber thickness measurements were obtained using ImageJ software (Fiji version 1.49q, National Institutes of Health, USA).

2.4. Cryogel production

2.5 mL of the homogenized suspension was poured into 24-well plates. The suspension was then ultra-frozen at −80 °C for 2 h and then lyophilized in a LyoMicron equipment (Coolvacuum, Spain). Once the cryogels were obtained, the plates were stored at 60 °C for 2 h to avoid contamination of the material until further use. Density was determined by measuring the mass of each sample with an analytical balance and calculating the volume from the geometric dimensions obtained with calipers. Porosity was quantified by the Brunauer-Emmett-Teller (BET) method following the procedure described by Méndez et al., 2023.

2.5. Compatibilization of cellulosic cryogels with PHA

Bacterial colonization methodology was adapted from the previous publication of Campano et al., 2022. The material development was mainly performed with mcl-PHA, subsequently the process was validated with an scl-PHA. Specifically, mcl-PHA monomer composition was 92–94 % of (*R*)-3-hydroxyoctanoic acid (HO) and 6–8 % of (*R*)-3-hydroxyhexanoic acid (HH) content. The mcl-PHA was produced in the recombinant *Pseudomonas putida* Pp08_225 strain, which is derived from the parental KT2440 strain, expressing the gene encoding the green fluorescent protein (*msfgfp*) driven by the BG42 promoter (Campano et al., 2022). This strains is named hereafter as *P. putida* GFP. Conversely, the strain *Pseudomonas putida* Pp00_02 was used to produce scl-PHA under the regulatory system $LacI^q$/Ptrc induced by IPTG. This is a KT2440 strain with the cluster *pha* deleted and with the genes of *phbABC* of *Cupriavidus necator* H16 for PHB production inserted in the chromosome (Manoli et al., 2023). This strains is named hereafter as *P. putida* ΔPHA-PHB.

A two-phase approach was proposed for cryogel-PHA compatibilization. The first phase, termed the colonization phase, involved a short period of time that allowed the cells to self-displace from the liquid phase into the cellulose cryogel. The second phase, called the proliferation phase, focused on promoting the growth and activity of the cell population that had previously colonized the material. The proliferation phase would involve an increase in the number of cells and, consequently, an increase in the proportion of PHA in the materials.

2.5.1. Colonization phase

Briefly, a pre-inoculum of *P. putida* GFP (mcl-PHA) or *P. putida* ΔPHA-PHB (scl-PHA) was prepared inoculating a colony in LB (Luria-Bertani) media at 200 rpm, 30 °C for 16 h. Then, the culture was washed with saline solution (0.9 % NaCl) and the cells were concentrated using M63 0.1 N nitrogen-limited minimal medium without carbon source. The M63 0.1 N media was prepared according to Manoli et al., 2023. Later, the suspension was used to adjust the concentration to 0.3 OD (at 600 nm) in flasks with M63 0.1 N media with sodium octanoate as carbon source to favor PHA accumulation. Specifically, for scl-PHA production using *P. putida* ΔPHA-PHB, kanamycin (50 μg/mL) and IPTG (1 mM) were added to the media.

The cultures were incubated at 200 rpm, 30 °C for 24 h. The accumulation of PHA granules within the cells was checked by light microscopy with a Leica DM4 B epifluorescence microscope (Wetzlar, Germany). The culture was then centrifuged and washed with saline (0.85 % NaCl) to prepare the inoculum for colonization experiments. The concentrated cell suspension was then used to adjust the optical

density (OD) to 0.9 at 600 nm in flasks containing 0.1 N M63 medium with or without carbon source to promote or discourage bacterial growth. Two milliliters of the cell suspension were added to each sample in the 24-well plate containing the cryogels. The plates were then incubated at room temperature for 2 h under static or shaking conditions. Subsequently, the cryogels were washed with 0.85 % NaCl solution and placed in HCl solution with the pH adjusted to 2.5 for 16 h. The cryogels were then washed with 0.85 % NaCl solution and placed in HCl solution with the pH adjusted to 2.5 for 16 h. The cryogels were then washed again with 0.85 % NaCl solution to neutral pH and finally lyophilized.

2.5.2. Proliferation phase

To obtain the proliferated materials, the colonized materials obtained in the previous section before acid treatment were used. Thus, after the 2 h of incubation, the cryogels were washed with 0.85 % NaCl and subsequently placed in flasks with 10 mL of 0.1 N M63 with 15 mM sodium octanoate as a carbon source to promote cell growth. In addition, in the production of scl-PHA, 1 mM IPTG was added to the M63 0.1 N culture medium. They were then incubated at 200 rpm at 30 °C for 16 h. Subsequently, the cryogels were washed, acidified and dried as mentioned in the previous section.

2.6. Cryogel characterization

2.6.1. Cryogel visual appearance

Digital images were acquired using an EVOCAM-II macroscope (Vision Engineering, Woking, UK). Images were acquired using VuPlus v1.00.82 software (2018, Vision Engineering, UK) and analyzed using Nis Elements BR 3.2 software (Nikon Corporation, Japan).

2.6.2. Counting viable cells that colonized the cryogels

Plate counts of the inoculum and viable cells within the materials were performed on LB agar plates. The inoculum was seeded directly from the liquid medium at various dilutions. The materials were first digested with cellulase to dissolve the matrix, and then the cells were seeded. Thus, the colonized cryogels (before the acidification process) were digested using cellulase from *Trichoderma reesei* (100 μL) and 0.05 M citrate buffer pH 4.8 (900 μL) at 30 °C and 200 rpm, until complete hydrolysis of the cellulose, as performed by Campano et al., 2022.

2.6.3. PHA quantification

The methodology employed for the extraction of PHA from cryogels involved several steps. First, Pyrex tubes were prepared by washing, drying, equilibration and weighing. Caps with rubber stoppers were used to prevent solvent evaporation. The cryogels were then dried at 60 °C for 2 h to remove excess moisture without damaging their composition. Subsequently, the cryogels were immersed in 3 mL of chloroform and kept at 80 °C for 3 h (Rodrigues et al., 2022). The cryogel was then removed and the chloroform was evaporated. The weight change of the tube was determined using an analytical balance, and the final weight gain was considered the mass of PHA extracted from the cryogel.

The content of the monomeric PHA composition was determined by gas chromatography–mass spectrometry (GC–MS) of the methanolized cryogel in a manner similar to De Eugenio et al., 2010. The methanolysis procedure was carried out by suspending 4–5 mg of the materials in 2 mL of methanol containing 15 % H_2SO_4 (3 % for PHB samples) and 2 mL of chloroform containing 0.5 mg/mL 3-methylbenzoic acid (internal standard). Then, the screw-capped tubes were incubated at 100 °C for 5 h. After cooling in an ice bath, 1 mL of deionized water was added, mixed manually and centrifuged at 3800 rpm, 4 °C for 10 min. The upper phase was then discarded and 1 mL of deionized water was added. The mixture was centrifuged again and the upper phase was also discarded. Subsequently, 0.1 g Na2SO4 was added to absorb the remaining water. After the two-step extraction process, the organic phase containing the resulting monomer methyl esters was analyzed by GC–MS. A standard curve of 0.5 to 2 mg P(3HB) was used to interpolate the sample data.

The analyses were performed on an Agilent 5975C (Waldbronn, Germany) coupled to an MS7890A (EI, 70 eV) and a split-splitless injector. 1 μL of the organic phase was injected into the GC at a split ratio of 1:50. The column used was an Agilent 122–5731 (400 °C: 30 m × 250 μm × 0.1 μm). With an initial temperature of 85 °C for PHA and 60 °C for PHB. Then at 115 °C (rate of 5 °C/min) for PHA and at 125 °C (rate of 10 °C/min) to allow efficient peak separation. Mass spectra were compared using the NIST database.

2.6.4. Confocal laser scanning microscopy (CLSM)

To analyze the internal structure of the cryogels, they were flash-frozen at −80 °C and then cut using a cryotome. The cryogels were glued to the base using Tissue-Tek O.C.T^{TM} embedding medium in a perpendicular position. The cryogels were then polished with the blade up to halfway with 60 μm steps at −23 °C. They were then stored at 4 °C until microscopic observation.

The internal structure of the cryogels was visualized using a Leica TCS SP5 confocal microscope. To enhance visualization of specific components, they were specifically stained. Cellulose was stained with 100 μL of a 35 μg/mL Calcofluor White M2R, while PHA particles were stained with 50 μL of a 2.5 μg/mL BODIPY. Images were acquired at 20× magnification with a step size of 5 μm until the signal became undetectable. To ensure optimal resolution and deep penetration into the sample, laser intensity and detector gain were adjusted during image acquisition. This approach ensured effective observation of the entire thickness of the cryogel section.

The CLSM image stacks were reconstructed into 3D representations to quantify the proportion of mcl-PHA in the samples. ImageJ software (Fiji version 1.49q, National Institutes of Health, USA) was used for image processing and analysis. Image stacks were 8-bit grayscale with two separate channels (blue (cellulose) and green (mcl-PHA)). Each stack had a frame size of 1024 × 1024 pixels, a field of view of 0.775 × 0.775 mm (pixel resolution of 0.757 μm) and included slices (from 26 to 47) and a voxel size of 2.86 cubic microns. Image processing and analysis was performed in three steps. First, sub-stack creation, to ensure a consistent sample volume in all conditions, a sub-stack containing 26 closest slices was generated for each original stack. Second, stack intensity normalization to compensate for possible loss of intensity due to increased depth within the sample, a stack intensity normalization was performed using the contrast processing tool. A uniform value of 0.4 % was applied to all stacks. Finally, volume analysis in which the volume of each color channel was analyzed independently using the 3D objects counter tool. Uniform threshold and minimum size values were applied for both channels. The total volume analyzed was 0.078 mm^3. Finally, the ratio of PHA granule volume to cellulose fiber volume was calculated to assess the relative abundance of PHA compared to cellulose.

2.6.5. Scanning electron microscopy (SEM)

The morphology of the cryogels was additionally observed by scanning electron microscopy (SEM) according to Rivero-Buceta et al., 2020, with minor modifications. Images were acquired using a Hitachi Model S-8000 with field emission filament (Tokyo, Japan) at an accelerating voltage of 3 keV. Prior to analysis, the samples were sputter-coated with gold using a Polaron SC7640 from Quorum Technologies Ltd. (Lewes, UK). In addition, elemental analysis by Energy Dispersive X-Ray Spectroscopy (EDXS) was performed on the control samples (cellulose cryogels only) to verify the presence of inorganic elements.

2.6.6. Water vapor sorption capacity (WVSC)

The dried materials were heated at 60 °C for 2 h and then equilibrated in a desiccator with silica gel to keep the cryogels away from water vapor. Subsequently, the samples were weighed using an analytical balance (Mettler Toledo, Spain). The cryogels were then placed in a

100 % relative humidity environment (inside a desiccator with distilled water at the bottom) and weighed at 8 and 15 days (Barroca et al., 2013). The difference in weight was assigned to the water vapor content absorbed by the material normalized by the weight of each sample.

2.6.7. Compressibility

Compression tests of the cryogels were performed with an INSTRON 34TM-5 (Instron Corporation, USA) double-column benchtop model with a strain rate of 5 mm/min. Peak force values were detected starting at 0.05 N using a compression deformation test. The parallel plate fixture was used, and measurements were performed at the temperature of 22 ± 2 °C and 60 ± 5 % relative humidity. At least three specimens were tested to ensure the accuracy of the measured data.

2.6.8. Thermogravimetric analysis (TGA)

Thermogravimetric analysis (TGA) was performed with a TGA 550 instrument (TA Instruments, USA). Samples were heated from 30 °C to 850 °C at a heating rate of 20 °C/min in air atmosphere. Derived thermogravimetric curves (DTG) were used to analyze weight loss events as a function of temperature. Percent ash content was determined as the sample residue remaining after completion of the temperature program.

2.6.9. Fourier-transform infrared spectroscopy (FTIR)

FTIR analyses were performed in the attenuated total reflectance (ATR) mode using Thermo Nicolet Nexus equipment (GMI, USA). Samples were placed on the ATR crystal for analysis at room temperature (22 ± 2 °C), and scans were performed with a resolution of 4 cm^{-1} in the spectral range of 4000–600 cm^{-1} and averaging a minimum of 32 scans, similar to de Oliveira et al., 2019.

2.6.10. Statistical analysis

All data were collected in triplicate. To assess significant differences between groups, a one-way Analysis of Variance (ANOVA) was performed, followed by a Tukey's honestly significant difference (HSD) post-hoc test. Statistical analyses were performed with Statgraphics 19 × 64 software (Statgraphics Technologies, USA).

3. Results and discussion

3.1. Composition analysis of the cellulose-rich fraction

RS cellulose, a promising candidate for absorbent materials, was used to develop the cryogels. The results shown in Fig. 1A demonstrate an increase in the percentage of cellulose after the various purification steps, with an extraction yield of 26.0 ± 5.8 %, while hemicellulose and lignin contents decrease. The presence of hemicelluloses in the fibers is of special interest in CNF production because they act as a barrier to microfiber aggregation during the homogenization process (Morcillo-Martín et al., 2022). A detailed characterization of the fractions and monosaccharides analyzed can be found in detail in Table S1 and Fig. S1. The lignin content was not completely removed during the treatments, which offers some advantages for the final material, as residual lignin can promote the formation of hydrogen bonds, improving the barrier properties and increasing the technical stability of cellulose fibers (Nair et al., 2017). In addition, lignin can impart hydrophobicity, antibacterial properties, antioxidant and UV stabilization (Wen et al., 2019).

FTIR analysis, shown in Fig. 1B, revealed changes in the chemical composition of the cellulosic extract compared to RS. The decrease or absence of specific peaks indicated satisfactory removal of impurities. The presence of the O—H stretching peak at 3306 cm^{-1} in both samples

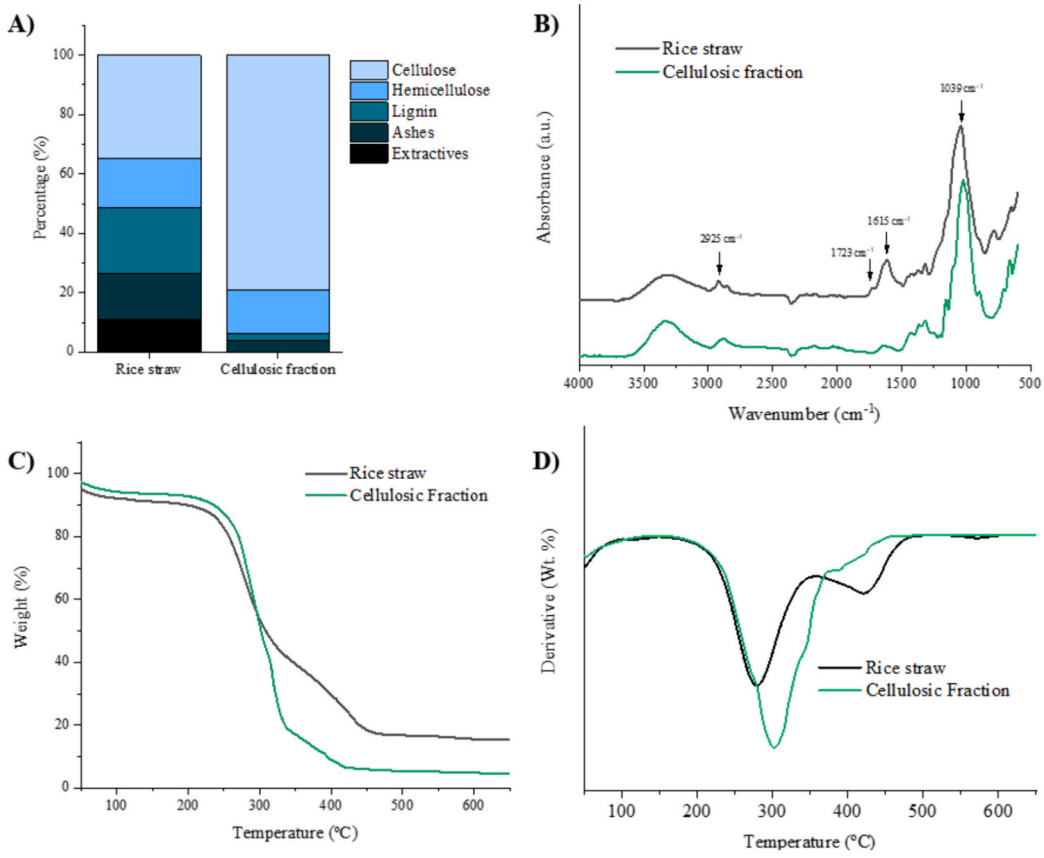

Fig. 1. Characterization of rice straw (RS) and cellulosic fraction (CF). A) Composition of cellulose, hemicellulose, and lignin in the RS and CF obtained by ion exchange chromatography and TAPPI T222 standard. B) FTIR spectra of the RS and the CF. The key peak changes are indicated by black arrows. C) Thermogravimetric analysis (TGA) curves and (D) Differential thermogravimetric analysis (DTGA) curves of the RS and the CF.

confirmed the existence of hydroxyl groups, a key functional group in cellulose. Significant spectral differences between RS and the cellulosic fraction indicated substantial compositional changes. For example, the C—H stretching peak (2925 cm^{-1}) characteristic of cellulose was mainly observed in the cellulosic fraction, suggesting cellulose enrichment after purification. The decrease or absence of specific peaks indicated the successful removal of impurities: a reduction of peak intensity between 2000 and 1750 cm^{-1} (attributed to lignin-associated structures) (Rodsamran & Sothornvit, 2015), the absence of peaks around 1750–1700 cm^{-1} (linked to hemicellulose and lignin), and the disappearance of peaks at 1615 cm^{-1} (C═O stretching of lignin) and 1723 cm^{-1} (C═O stretching of the ester group in hemicellulose and lignin) in the cellulosic fraction. Furthermore, in the 1700–1600 cm^{-1} region, the increase of the 1615 cm^{-1} peak in F3 could possibly be attributed to oxidation caused by NaClO2 treatment. While the 1039 cm^{-1} peak indicated residual hemicellulose (specifically xylan) in all fractions, a significant reduction in intensity was observed in the 1000–980 cm^{-1} region (C—C, C—O, C—H stretching and C-OH bending in cellulose) after the extraction procedure, thus confirming the suitability of the purification method.

Further analysis of RS and the cellulosic fraction was carried out by thermogravimetric analysis (TGA), and the results are presented in Fig. 1C and D. The TGA curves revealed a thermal profile shift in the cellulosic fraction, typically associated with cellulose degradation (280–380 °C) (Díez et al., 2020). In detail, it has been described that the degradation process is sequential, with typical degradation temperature ranges in air of 250–300 °C for hemicelluloses, 300–350 °C for cellulose and 300–500 °C for lignin (Carrier et al., 2011). As seen in Fig. 1C-D, both samples revealed an initial weight loss at 100 °C, corresponding to water removal, followed by a significant weight loss at 300 °C, which can be attributed to cellulose degradation. The purified cellulosic fraction sample exhibited a more pronounced peak, corroborating the compositional analysis indicating a higher cellulose content in this fraction. Similarly, the reduction of the peak at 400 °C suggests a reduction of the lignin content in the final fraction. These results collectively support the success of lignin and hemicelluloses reduction during rice straw processing. The cellulose-rich fraction, with its residual lignin content, was used for further processing, including oxidative chemical stabilization, high-pressure homogenization, and cryogel fabrication.

3.2. Chemical modification and production of cellulose cryogels

Porous cellulosic materials sometimes have limited application in high humidity environments due to their inherent fiber separation by water (Lindman et al., 2010). This necessitates the development of more stable networks with higher cross-linking and strength. In this study, CNFs were produced using TEMPO-mediated oxidation pretreatment to facilitate fiber separation during high-pressure homogenization (Wen et al., 2019).

Previous studies have shown that these CNFs mostly retain their uniform hydrogen bonding cross-linked configuration after freeze-drying (Jiang et al., 2020). Oxidation increases the anionic charge on the cellulose surface, promoting electrostatic repulsion between fibrils and facilitating fibrillation, diameter reduction and increased surface area interaction (Balea et al., 2020). The degree of oxidation, quantified by carboxylic acid content, was 0.24 mmol/g for the initial cellulosic fraction and 0.34 mmol/g for the oxidized pulp. These results agree with the previous report by Isogai et al., 2011 indicating a sufficient degree of oxidation to induce efficient fibrillation. To evaluate the benefits of oxidation in HPH for cellulose fiber separation, the unoxidized cellulosic fraction was subjected to HPH followed by lyophilization. Unoxidized cellulose minimally inhibited size reduction or fiber separation after HPH (Fig. 2A). In contrast, oxidized cellulose showed a significant decrease in diameter and length after HPH treatment. In addition, oxidized cryogels showed superior structural firmness (non-dispersible materials) in water compared to their non-oxidized counterparts, maintaining their structural integrity after immersion (Fig. 2B).

The impact of high pressure homogenization passes on cellulosic suspension gels was studied. The suspension gel appearance was directly proportional to the number of passes studied (2, 4 and 8 HPH passes), suggesting a potential reduction of fiber diameter at the micro- or nanometer scale. After freeze-drying the different oxidized-homogenized suspensions, the cryogels maintained structural integrity even after immersion in water, indicating the stability of the fabricated materials.

In addition, SEM analysis revealed significant structural variations with HPH treatment (Fig. 2C). Treatments 2 and 4 HPH showed trends towards larger pores and irregular structures. In contrast, treatment 8 HPH showed well-defined lamellar structures with small pores. These structures probably arose from the collapse of nanofibrils during freeze-drying due to water crystal formation. The higher degree of CNF

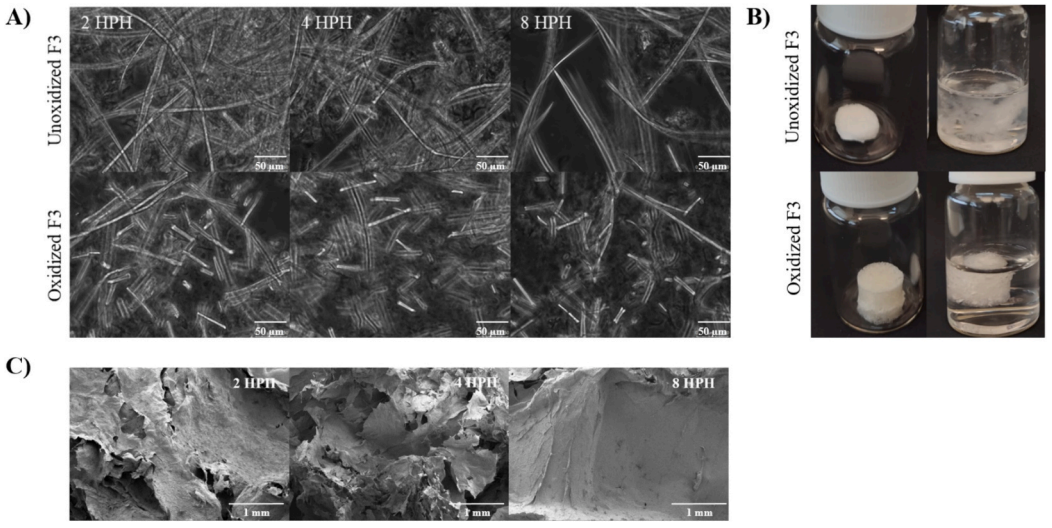

Fig. 2. A) Polarized light microscopy images of the homogenized suspensions for both oxidized and unoxidized cellulosic fraction (F3). The effect of high-pressure homogenization after 2, 4 and 8 HPH passes is shown. B) Pictures of unoxidized and oxidized cryogels. Left: cryogels in their dry state. Right: cryogels after immersion in water. C) Scanning electron microscopy of the cryogels obtained by freeze-drying the suspension after 2, 4 and 8 high-pressure homogenization (HPH) passes.

fibrillation with HPH passes may have resulted in a denser network with smaller pores, which could hinder water outflow during drying. Previous studies attributed the self-assembly of CNF into macroscopic submicron fibers during freeze-drying to ice crystal tempering (Jiang et al., 2013). This lamellar structure, with microporous internal cavities and active walls provided by carboxyl groups, suggests a potential to facilitate the attachment of both PHA-producing bacteria and PHA particles.

Despite the nanometer size of the CNF thickness, which was observed to be 65.1 ± 25.40 nm in the TEM microscopy images (Figs. S7 and S8), the material subjected to 8 passes of HPH was found to be the only one that allowed the BET area to be measured, as other materials had significantly higher porosity and failed to retain nitrogen. The specific BET area of the tested material was determined to be 5.67 m^2/g. Similar values were obtained from Sehaqui et al., 2010, where the authors explained that BET values are low because during the freeze-drying sublimation process individual CNFs can aggregate by formation of physical bonds between fibers (van der Waals and hydrogen bonds).

3.3. Cryogel compatibilization with mcl-PHA

Next, live bacteria were used as PHA carriers to introduce them into the pores of the cellulosic cryogels, with the aim of making the materials compatible. Thus, motile bacterial cells were brought into contact with the porous cellulosic cryogels, which colonized the entire scaffold and were trapped inside. After colonization, the material was incubated in a fresh medium with carbon source for further PHA accumulation and bacterial proliferation. Subsequently, PHA was released from the disaggregated cells after immersion in acid in which the physical interaction of PHA with cellulose fibers was favored. The following subsections will discuss the efficacy of these treatments in terms of the most suitable conditions for maximum PHA accumulation in the materials.

3.3.1. Optimizing bacterial colonization of cryogels for reduced energy consumption

The objective of this section was to optimize bacterial colonization in cryogels with the lowest resource consumption. We hypothesized that static incubation without carbon source would be the most energy efficient method. Importantly, this approach relies on bacterial motility, so there is no need to increase cell biomass (cell growth), but the cells need energy to swim through the cryogel, which could involve catabolization of the carbon source. The experiments investigated the effects of incubation type (static vs. agitated) and the presence/absence of a carbon source on colonization efficiency (Fig. S2). In particular, within the 2-hour incubation period tested, no significant differences were observed between static and agitated incubation, neither with the use of a carbon source or variation of inoculum concentrations. Based on these results, a 2-hour static colonization procedure without a carbon source was chosen. This approach minimizes the overall carbon source requirement, leading to a more efficient process. In addition, the short incubation time ensures mobilization of cells into the material before they begin to consume their own PHA reserves for energy. As highlighted by (Manoli et al., 2022), PHA serves as a carbon and energy reserve for bacteria during periods of starvation. Minimizing PHA consumption during the colonization process translates into a reduction of the final amount of polymer deposited within the cryogel, further contributing to resource efficiency. Although inoculum concentration did not have a significant impact on colonization in this study, PHA content per cell will be key for maximum deposition.

3.3.2. Comparative evaluation of viable cell retention capacity

To investigate the effect of porosity, the materials were evaluated with 2, 4 and 8 HPH under the previously determined conditions of no carbon source and static incubation for 2 h. For this purpose, the colonization of cryogels with 2, 4 and 8 HPH passes was compared using an inoculum of 0.9 OD (5–5.7 log CFU/ml). Fig. 3 shows the inoculum for each case and the number of bacteria deposited on the material after

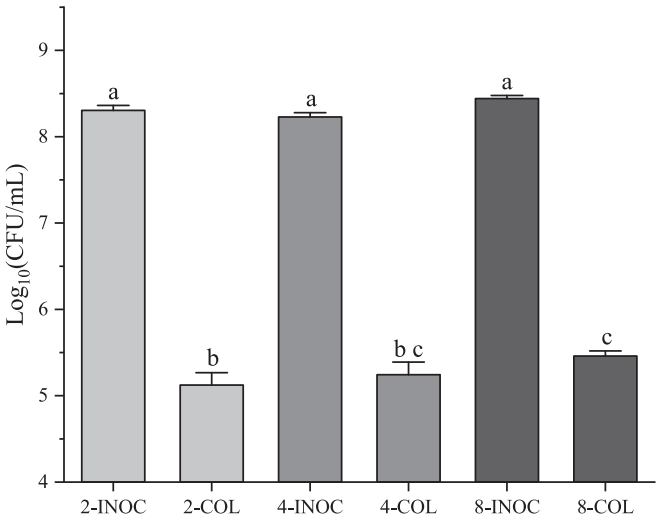

Fig. 3. Plate count in Colony Forming Units per milliliter (CFU/mL) of the inoculum (INOC) and bacteria that colonized the material (COL). The INOC values represent the count of cells in the liquid culture (inoculum), while the COL values were obtained through digestion of the material with cellulases followed by counting, representing the proportion of bacteria inside the material. 2, 4 and 8 numbers represent the number of high-pressure homogenization passes. Different letters (a,b and c) represent significant differences at $p < 0.05$ probability level.

colonization (COL). The results indicated that the number of bacteria deposited increased in cryogels made with a higher number of passes through the homogenizer, with significant differences observed between 2 and 8 passes through the HPH. However, there were no significant differences between 4 passes of HPH and the other treatments. When comparing the percentage of cells retained in each case relative to the initial inoculum, it was observed that 2 passes of HPH retained 62 % of the cells, 4 passes of HPH retained 64 % and 8 passes of HPH retained 65 % of the cells. Although the variations in cell counts were not statistically significant, possible differences in polymer deposition by porosity prompted further analysis in subsequent experiments. The 8-pass HPH material was selected for subsequent experiments as it appears to be more suitable for cell retention.

3.3.3. Colonization of cryogel by PHA-containing bacteria

Next, colonization of the materials was investigated using *P. putida* cells with accumulated PHA granules, as shown in Fig. S3. This procedure allowed the cells to migrate from the liquid medium to the inside of the submerged cryogel and subsequently settle around the cellulose fibers. Once the bacteria were placed around the fibers, the cells were lysed by mild acid treatment and the polymer remained attached to the cryogel, as previously demonstrated (Campano et al., 2022). This fact was further observed by CLSM, as shown in Fig. 4.

After performing a surface visualization, the need to determine the internal components of the materials was identified in order to assess the degree of bacterial penetration and thus the position of the PHA. Therefore, a cryotome was employed to create a cross section of the cryogel that could be observed by CLSM. As illustrated in Fig. 4B, the colonization of the 8-pass PHA material was more visible on the internal structure of the cryogel compared to that observed on the surface (Fig. 4A). Also, the effect of using different inoculum concentrations (0.3 and 0.9 OD) on granule deposition and pore potential saturation was evaluated to corroborate the relationship between inoculum concentration and porosity. The results in Fig. 4B suggest that the proportion of PHA deposited in the cryogel colonized by the 0.9 OD inoculum concentration was slightly higher than that of 0.3 OD. These results suggest that increasing the inoculum causes an increase in the PHA carrying capacity of the material. It is known that handling the cryogel and

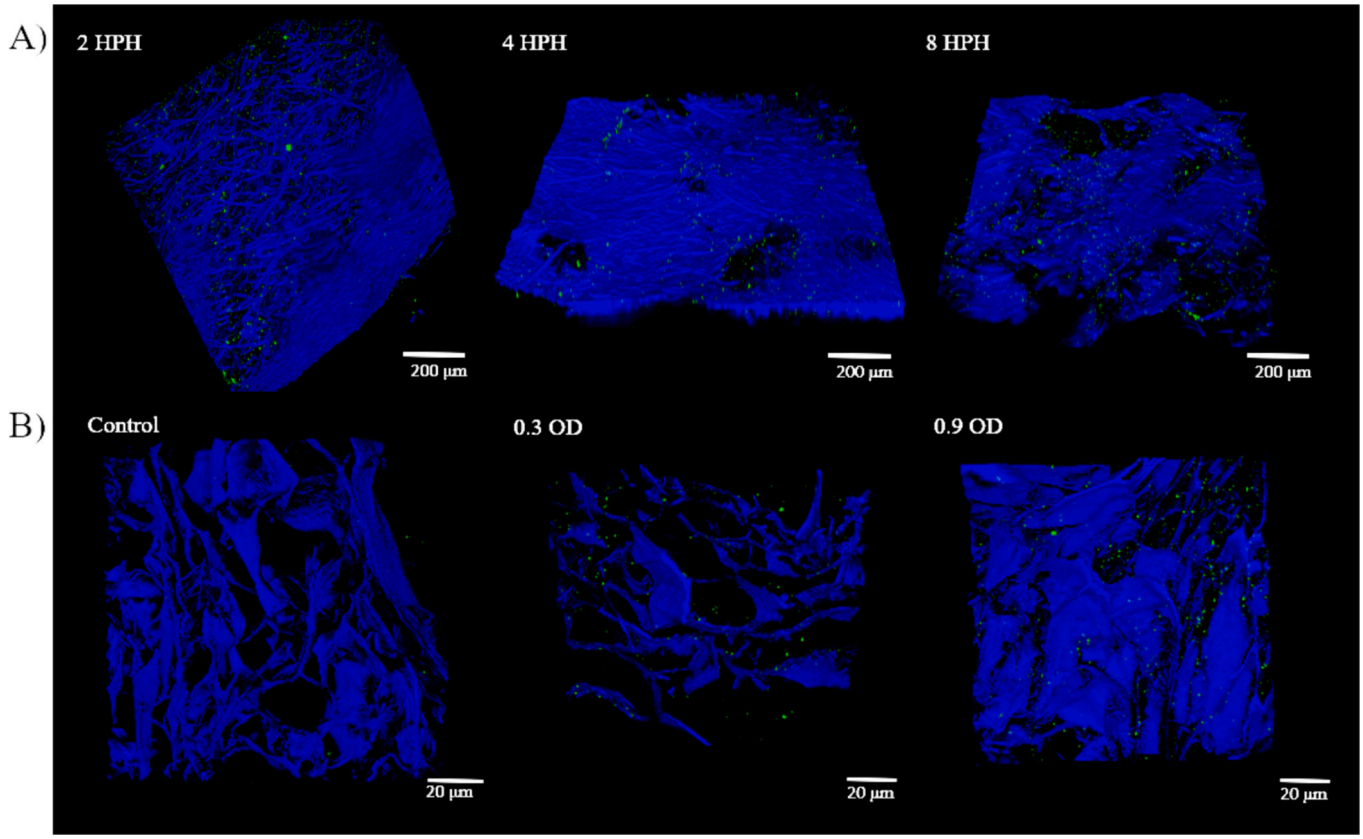

Fig. 4. A) 3D reconstruction of cryogels fabricated with 2, 4 and 8 HPH CNFs colonized with 0.9 OD. B) 3D reconstruction of 8 HDH cryogels colonized with 0.3 OD and 0.9 OD. The cellulose fibers and PHA granules were digitally colored in blue and green, respectively.

preparing the samples for analysis can lead to breakage or deformation of the structure, making it difficult to obtain accurate images (Aegerter et al., 2011). In this case, the structure of the developed materials was preserved, even during the treatment applied for visualization.

3.3.4. *From colonization to proliferation*

After successful colonization of the cryogel with cells, our goal was to increase the PHA content within the material by promoting proliferation of the colonizing cells by providing a nutrient medium in which the bacteria could grow. Fig. 5 shows the 3D reconstruction of the CLSM images of the materials fabricated by colonization and proliferation in 2, 4 and 8 HPH passes. The left panel illustrates the colonized materials, where granules were observed to be attached to the surface of the material fibers. In contrast, the proliferated materials, shown in the right panel, exhibited a higher accumulation of PHA granules than the colonized ones. In addition, materials with 4 and 8 passes of PHA exhibited greater polymer accumulation.

3.4. *Impact of scl-PHA and mcl-PHA incorporation on cryogel properties: A comparative characterization*

This section aims to demonstrate the versatility of the technique using *P. putida* cells to incorporate different types of PHA into cellulose cryogels. This strain does not produce scl-PHA naturally, but has been genetically modified to generate many types of PHAs (Manoli et al., 2023). The effect of PHA type on the final material properties was investigated using scl-PHA and mcl-PHA producing bacteria (for details, see Materials and methods). Characterization focused on materials developed using the most suitable colonization and proliferation conditions established with the 8-pass HPH material, as previously described for mcl-PHA.

3.4.1. *PHA quantification*

Three complementary methods were used to quantify the amount of mcl-PHA and scl -PHA in the samples: chemical extraction with chloroform, image analysis and GC–MS methanolysis. While the first two methods provide an approximation to semi-quantify the amount of PHA deposited in the cryogel, the GC–MS data obtained after methanolysis provide accurate values, so they were used as a reference. As shown in Table 1, the proliferated samples for mcl-PHA and scl-PHA showed the same pattern, more PHA accumulated in the proliferated samples than in the colonized samples. In addition, the percentage of accumulated PHA was higher in mcl-PHA than in scl-PHA.

Secondly, according to the extraction results, the mcl-PHA content was also significantly higher in the proliferated material (4.44 ± 0.90 %) compared to the colonized one (0.68 ± 0.02 %), confirming the hypothesis of a higher mcl-PHA deposition in the proliferation process. On the other hand, the evaluation performed by image analysis revealed a value of 1.49 % and 0.11 % mcl-PHA content for the proliferated and colonized materials, respectively. A similar behavior was observed for the scl-PHA-modified materials, whose chloroform-mediated extraction revealed a significantly higher scl-PHA content (2.32 ± 0.66 %) in the proliferated material compared to the colonized material (1.67 ± 0.55 %). As can be concluded from these results, the mcl-PHA-modified cryogels exhibited a slightly higher PHA content than those functionalized with scl-PHA.

By combining these techniques, a more complete understanding of the composition of the cryogel can be achieved. In this case, it was corroborated by image analysis that the distribution of PHA in the cellulose matrix was not completely homogeneous, there being regions with a lower percentage of PHA, as is the case analyzed, and other regions with a higher proportion of this bacterial biopolymer. This suggests either a better compatibility between mcl-PHA and the cellulosic matrix, due to the more amorphous character of this type of PHA, or an

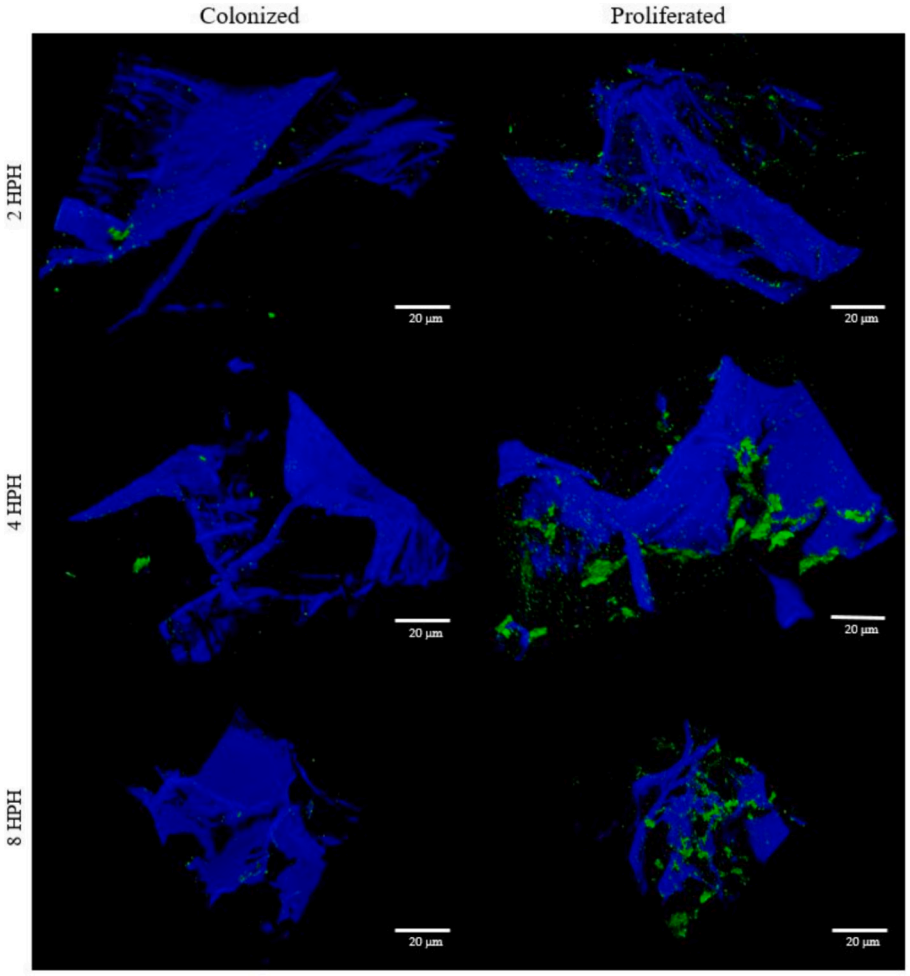

Fig. 5. 3D reconstruction of cryogel obtained by cutting with a cryotome to visualize the internal structure with confocal microscopy. The cryogels were colonized (COL) or subjected to proliferation (PROL). The numbers indicate the number of HPH passes 2, 4 or 8 on each case.

Table 1
Percentage of PHA measured in the colonized and proliferated cryogels under GC–MS and chloroform extraction.

Sample	PHA content (%)	
	GC–MS	Extraction
mcl-PHA COL	1.49 ± 0,23 [a]	0.68 ± 0.02 [a]
mcl-PHA PROL	4.09 ± 0.84 [b]	4.44 ± 0.90 [b]
scl-PHA COL	0.82 ± 0.09 [a]	1.67 ± 0.55 [c]
scl-PHA PROL	1.61 ± 0.60 [a]	2.32 ± 0.66 [c]

easier penetration of the mcl-PHA producer into the matrix compared to that of the scl-PHA producing strain.

In addition, FTIR spectroscopy was used to validate the previously quantified PHA content. This complementary technique provided valuable information on the chemical composition of the treated samples. Fig. 6A shows the FTIR spectra of the cryogels. The characteristic bands of PHA, which serve as a fingerprint of the presence or absence of PHA, were clearly observed. These bands include the stretching of the ester carbonyl (1700 to 1720 cm^{-1}) and the multiple bands between 1450 and 1000 cm^{-1} attributed to methyl (CH_3) and methylene (CH_2) deformations, as well as CO stretching (Kansiz et al., 2007; Porras et al., 2016). In agreement with Campano et al. (2022), the peak observed near 1650 cm^{-1} suggests the possible presence of residual lipids or proteins remaining in the cryogel despite washing procedures, thus indicating that some remaining cellular debris was present in the materials.

3.4.2. Thermogravimetric analysis TGA

The control sample exhibits a two-step thermal degradation process, as shown in Fig. 6B and C. The first step at 307 °C is attributed to cellulose degradation, while the second step at 420 °C is attributed to lignin (Kaur & Kuhad, 2019; Bradbury et al., 1979). In the 200–350 °C range, the incorporation of mcl- or scl- PHAs results in a shift towards lower degradation temperatures, indicating the presence of PHA, with lower thermal resistance (Ross et al., 2017). As reported by Luo et al., 2006, PHA degradation temperatures typically fall within the range of 218–235 °C, with a proportional increase in degradation temperature with increasing mol% of mcl-3HA. Consistent with these findings, Fig. 6C reveals a shoulder peak at approximately 261 °C, particularly evident in the proliferated sample, indicative of mcl-PHA degradation. In contrast, scl-PHA degradation appears as a shoulder peak at a slightly lower temperature (253–255 °C) and shows a greater presence in the proliferated material. These results corroborate that PHA incorporation affects the thermal properties of cryogels.

3.4.3. Macro and microscopic morphology

Macroscopic evaluation of the cryogel structure and the presence of PHA particles was performed using the 8-pass HPH material under both colonization and proliferation conditions. As illustrated in Fig. 7, the treated materials retained their structural integrity after the colonization procedure. In addition, the typical CNF cryogel structure was achieved. Previous authors reported for TEMPO-oxidized and high-pressure homogenized samples that the structure was typical of a mesoporous material and that CNFs would be acting as a basic framework

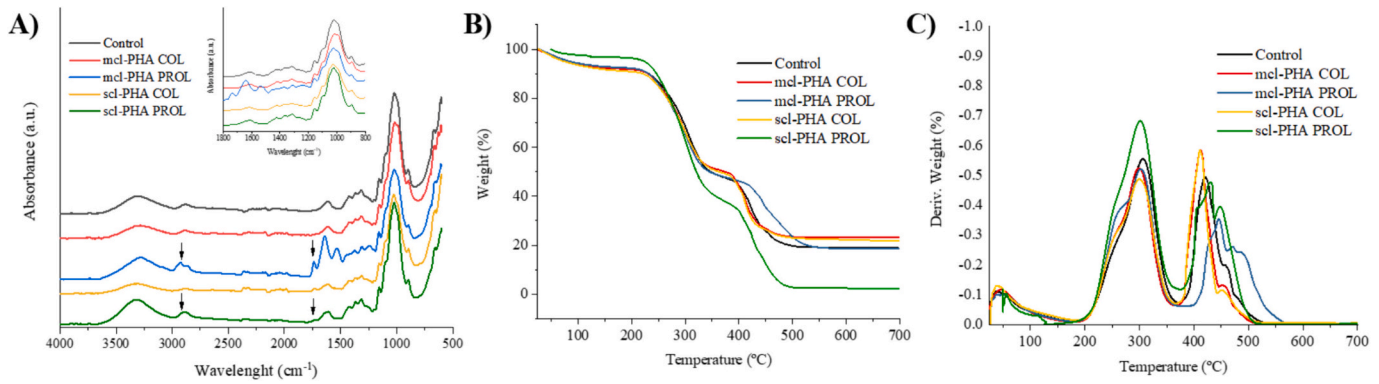

Fig. 6. A) FTIR spectra of the cryogels: control, colonized (COL), proliferated (PROL), treated with mcl-PHA or scl-PHA. B) TGA and C) DTGA curves of the cryogels: control, colonized (COL) and proliferated (PROL), treated with mcl-PHA and scl-PHA.

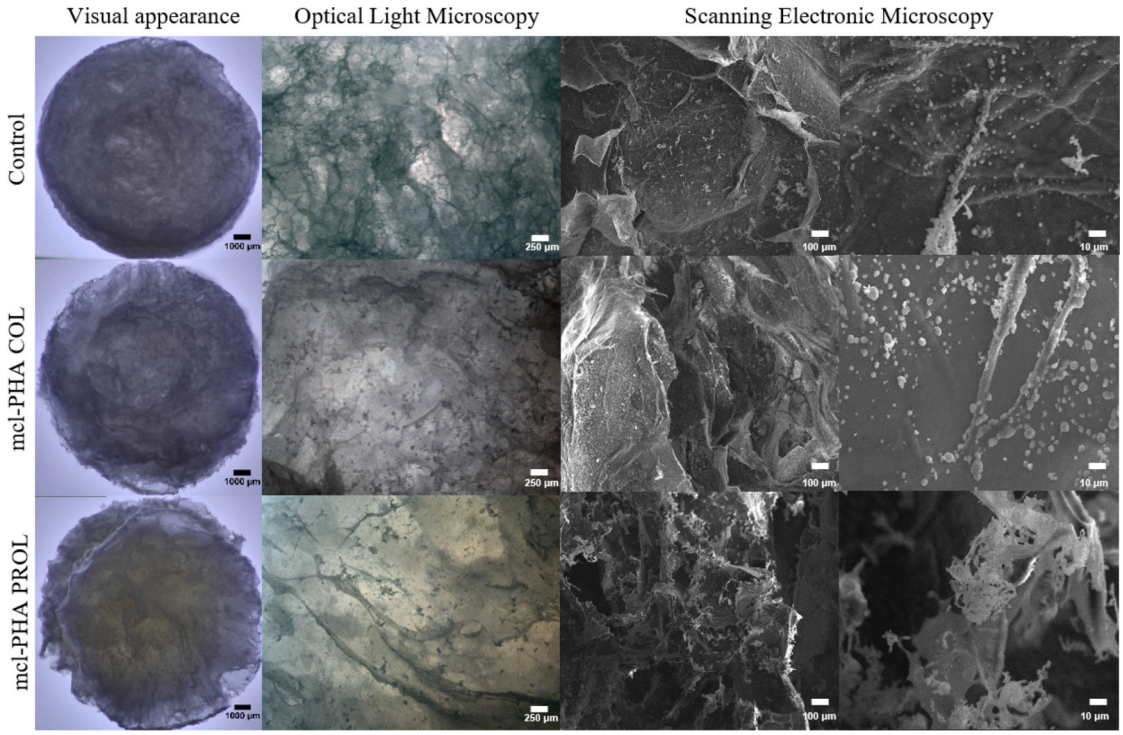

Fig. 7. Visual appearance, optical light microscopy and scanning electron microscopy (SEM) images of cryogels prepared using mcl-PHA. COL and PROL denote colonization and proliferation, respectively. Column 1: Overall structure of the cryogel at low magnification. Column 2: Magnified view (2×) to highlight the surface morphology of the cryogel. Columns 3 and 4: SEM images providing detailed information about the cryogel's microstructure. (Photographs of scl-PHA PROL and COL are shown in Supplementary Fig. S9).

surrounded by hydrogen bonds to form a strong structure (Wang et al., 2020). In addition, macrophotographs revealed the possible presence of PHA granules within the samples after colonization and proliferation treatments. Furthermore, no significant differences in density were observed between colonized and proliferated samples (see Table S2 for details).

To provide a detailed understanding of the microstructural changes, an SEM study of the developed materials was performed. Fig. S4 shows that the different materials presented different levels of porosity as a function of the number of HPH passes. The results also showed some agglomerations with different morphology depending on the sample. An Energy Dispersive X-Ray Spectroscopy (EDXS) analysis of these particles detected the presence of sodium and chlorine elements that could have remained inside the cryogels from the various chlorine-related treatments performed to the pulp (cf. Fig. S5 in the Supplementary Material).

Regarding the microstructure, a difference in pore size caused by the presence of each type of PHA is observed. In the case of the materials modified with mcl-PHA, a more laminar structure is presented, with larger cavities where the PHA is located in the form of aggregates. However, the materials composed of cellulose and scl-PHA present a more network structure, with a more inclined appearance, possibly due to the higher crystallinity of this polymer. In this case, the cavities present a smaller size where, in the same way, the PHA aggregates are located.

3.4.4. *Water vapor sorption capacity (WVSC)*

Water vapor sorption capacity (WVSC) was measured to evaluate the impact of PHA on cellulose cryogels. As shown in Fig. 8A, significant differences were observed when PHAs were incorporated at higher concentrations (mcl-PHA PROL, scl-PHA COL and scl-PHA PROL). In particular, the proliferated samples showed a decrease in WVSC, demonstrating that the cell-driven PHA deposition method effectively

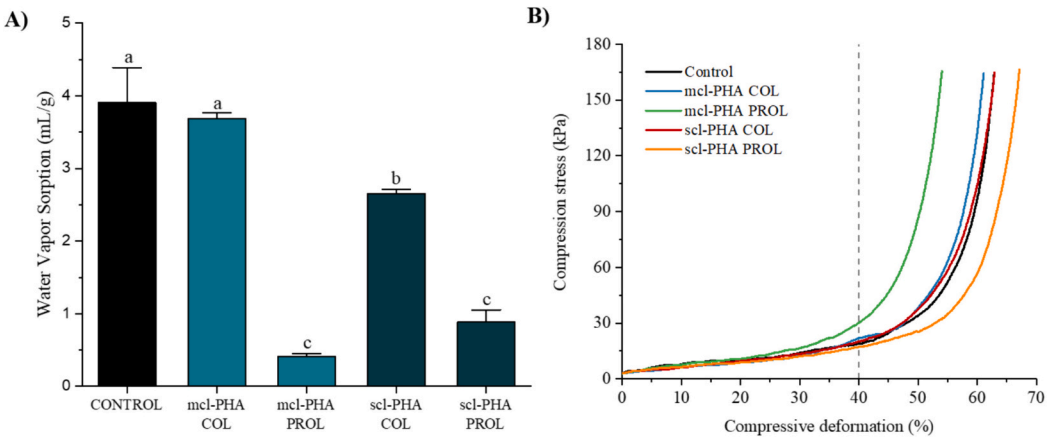

Fig. 8. A) Sorption of water in a closed environment with 100 % humidity after 8 days of exposure. The represented values showed the volume absorbed in mL before and after the PHA treatments. The abbreviations COL and PROL denote colonization and proliferation, respectively. B) Compressive deformation versus strength of the different cryogels tested by parallel plates with the Instron equipment.

enabled the deposition of PHA granules onto the cryogel, thus influencing the WVSC of the materials. This reduction in WVSC can be attributed to the decrease in cellulosic surface area available for interaction with water molecules, occupied instead by PHA granules. Furthermore, the effectiveness of the proliferated treatments in reducing water vapor sorption depended on the type of PHA deposited and the incubation time. Therefore, the use of different bacterial strains, PHA types and incubation times can be a tremendously useful tool to develop ad hoc materials with predetermined WVSCs. Some potential applications of these materials include the development of moisture-resistant packaging materials. The reduced WVSC makes these materials suitable for packaging moisture-sensitive products in humid environments, which could be especially beneficial for electronics or pharmaceutical packaging (Ciuffarin et al., 2023). In addition, these materials can be used to develop selective filtration membranes for water treatment or gas separation processes where controlled water vapor permeability is desired (Perera et al., 2023; Persano et al., 2024). The reduced moisture absorption can also be advantageous in the development of insulating materials; these cryogels can be used for thermal and acoustic insulation applications in buildings, especially in humid environments (Le et al., 2023). In addition, the ability to tailor water vapor sorption capacity could be valuable in the development of controlled release systems for active ingredients.

3.4.5. Compression test

Compression tests were performed to investigate the mechanical behavior of the cryogels. Images acquired before, during and after compression test have been included in Fig. S6. The average dimensions of the studied samples were a diameter of 10.93 ± 0.68 mm, a height of 4.67 ± 0.73 mm, and a volume of 440 ± 80 mm^3. As shown in Fig. 8B, significant differences were observed between the control sample and those incorporating mcl-PHA and scl-PHA. The material proliferated with mcl-PHA, due to its higher PHA content, showed the highest compressive strength compared to the other samples. This was particularly evident at 40 % compressive strain, where the strain values were: 18.78 kPa (control), 21.96 kPa (colonized mcl-PHA), 30.23 kPa (proliferated mcl-PHA), 20.05 kPa (colonized scl-PHA) and 17.18 kPa (proliferated scl-PHA). colonized mcl-PHA produced a modest increase in compressive strength compared to the control. This effect further increased with a higher degree of mcl-PHA incorporation. Consistent with previous findings, in which PLA coating improved the mechanical properties of cellulose cryogels (Benito-González et al., 2020), materials with mcl-PHA showed a slight improvement in compressive strength. In contrast, the incorporation of scl-PHA did not improve the mechanical properties and even led to an increase in brittleness, probably attributed to the higher crystallinity regions of scl-PHA (Silva et al., 2021) and the previously reported high brittleness (Wang et al., 2016). Furthermore, scl-PHA is mainly characterized by stiffness and brittleness, whereas mcl-PHA is defined by high flexibility and low stiffness (Panaitescu et al., 2016).

As shown in Table 2, the incorporation of different PHAs did not significantly affect the Young's modulus of the materials, indicating that their elasticity remains unchanged despite alterations in water vapor sorption functionality. Comparison with other cellulose-based aerogels and cryogels revealed similar Young's modulus values, typically ranging from 1 to 10 MPa (Sescousse et al., 2011). Cellulose cryogels, modeled as non-ideal open-cell foams, have a modulus between 2.5 and 3 MPa due to thicker pore walls formed during freeze-drying, resulting in higher values compared to cellulosic aerogels. Our materials showed a Young's modulus higher than previously recorded for cryogels and within the range of aerogels.

4. Conclusion

In conclusion, our research outlined an innovative methodology for the development of CNF-PHA cryogels by live cell-mediated PHA deposition, showing a remarkable reduction of their sorption capacity up to 6-fold with a low PHA integration ratio (2–4 %). The efficiency of the process was found to be dependent on the amount of PHA used. Thus, the amount of PHA deposited in the cryogels was modulated by the inoculum concentration, bacterial strain, colonization conditions and cell proliferation within the material. Surprisingly, the process achieved a significant reduction in water sorption capacity, without impairing the density or elasticity of the cryogels. In addition, the compressive strength showed a relationship with the type of PHA used, with slightly higher strength observed in the mcl-PHA-modified materials and higher deformation in the scl-PHA-modified ones. The versatility of this method was further evidenced by its adaptability to various

Table 2
Young's modulus for mcl-PHA and scl-PHA samples, as well as control, colonized (COL) and proliferated (PROL) treatments. Different uppercase letters indicate statistically significant differences after ANOVA and Tukey-HSD analyses.

Sample	Young's Modulus (Mpa)
Control	6.52 ± 0.48 ^{a}
mcl-PHA COL	6.40 ± 0.56 ^{a}
mcl-PHA PROL	6.55 ± 0.31 ^{a}
scl-PHA COL	5.73 ± 0.31 ^{a}
scl-PHA PROL	6.21 ± 0.21 ^{a}

bacterial strains and PHA types, including mcl-PHA and scl-PHA, and its ability to fine-tune PHA deposition by controlled incubation times. The efficacy of our proposed technique is manifested by reducing the surface area exposed to water vapor in the cellulose matrix through coverage with PHA granules both internally and externally, establishing a novel design approach for materials science that can meet specific functional requirements. Unlike conventional coating processes, this bacteria-mediated strategy allows complete penetration of the polymer into the cryogel matrix, facilitated by bacterial motility that ensures complete internal coverage. This approach not only introduces an avenue to generate cryogels with the desired water vapor sorption capacity, but opens up the possibility of developing potential functional properties by employing functionalized PHA variants and underscores the potential of this technique to advance materials design and applications.

CRediT authorship contribution statement

Laura Cabrera-Villamizar: Writing – original draft, Methodology, Investigation, Formal analysis, Data curation, Conceptualization. **Cristina Campano:** Writing – review & editing, Supervision, Methodology, Investigation, Formal analysis, Data curation, Conceptualization. **Amparo López-Rubio:** Writing – review & editing, Supervision, Resources, Project administration, Funding acquisition, Conceptualization. **María José Fabra:** Writing – review & editing, Validation, Supervision, Resources, Project administration, Funding acquisition, Formal analysis, Conceptualization. **M. Auxiliadora Prieto:** Writing – review & editing, Validation, Supervision, Resources, Project administration, Investigation, Funding acquisition, Conceptualization.

Declaration of competing interest

The authors declare that they have no known competing financial interests or personal relationships that could have appeared to influence the work reported in this paper.

Data availability

Data will be made available on request.

Acknowledgements

Grants PID2020-112766RB-C21, PID2020-112766RB-C22 and PCI2024-153409 funded by MICIU/AEI/ 10.13039/501100011033 and, by ERDF A way of making Europe. Laura Cabrera-Villamizar acknowledges financial support from the Generalitat Valenciana for the award of a Santiago Grisolía grant (GRISOLIA/2021/050). The Accreditation as Center of Excellence Severo Ochoa CEX2021-001189-S funded by MCIN/AEI / 10.13039/501100011033 is also fully acknowledged. The authors would like to thank Jose María Coll for his help in processing the confocal laser scanning microscopy images.

Appendix A. Supplementary data

Supplementary data to this article can be found online at https://doi.org/10.1016/j.carbpol.2024.122604.

References

Aegerter, M., Leventis, N., & Koebel, M. (2011). *Aerogels handbook (Advances in Sol-Gel 401 Derived Materials and Technologies)* (p. 932). Springer.
Balea, A., Fuente, E., Monte, M. C., Merayo, N., Campano, C., Negro, C., & Blanco, A. (2020). Industrial application of nanocelluloses in papermaking: A review of challenges, technical solutions, and market perspectives. *Molecules, 25*(3), 526.
Bandara, N., & Wu, J. (2018). Chemically modified canola protein–nanomaterial hybrid adhesive shows improved adhesion and water resistance. *ACS Sustainable Chemistry & Engineering, 6*(1), 1152–1161.
Barroca, N., Borges, L. M., Velez, F. J., Monteiro, F., Górski, M., & Castro-Gomes, J. (2013). Wireless sensor networks for temperature and humidity monitoring within concrete structures. *Construction and Building Materials, 40*, 1156–1166.
Benito-González, I., del Mar Ortiz-Gimeno, M., López-Rubio, A., Martínez-Abad, A., Garrido-Fernández, A., & Martínez-Sanz, M. (2022). Sustainable starch biocomposite films fully-based on white rice (Oryza sativa) agroindustrial by-products. *Food and Bioproducts Processing, 136*, 47–58.
Benito-González, I., López-Rubio, A., Gómez-Mascaraque, L. G., & Martínez-Sanz, M. (2020). PLA coating improves the performance of renewable adsorbent pads based on cellulosic aerogels from aquatic waste biomass. *Chemical Engineering Journal, 390*, Article 124607.
Besbes, I., Alila, S., & Boufi, S. (2011). Nanofibrillated cellulose from TEMPO-oxidized eucalyptus fibres: Effect of the carboxyl content. *Carbohydrate Polymers, 84*(3), 975–983.
Bradbury, A. G., Sakai, Y., & Shafizadeh, F. (1979). A kinetic model for pyrolysis of cellulose. *Journal of applied polymer science, 23*(11), 3271–3280.
Campano, C., Rivero-Buceta, V., Fabra, M. J., & Prieto, M. A. (2022). Gaining control of bacterial cellulose colonization by polyhydroxyalkanoate-producing microorganisms to develop bioplasticized ultrathin films. *International Journal of Biological Macromolecules, 223*, 1495–1505.
Carrier, M., Loppinet-Serani, A., Denux, D., Lasnier, J. M., Ham-Pichavant, F., Cansell, F., & Aymonier, C. (2011). Thermogravimetric analysis as a new method to determine the lignocellulosic composition of biomass. *Biomass and Bioenergy, 35*(1), 298–307.
Cebrián-Lloret, V., Metz, M., Martínez-Abad, A., Knutsen, S. H., Ballance, S., López-Rubio, A., & Martínez-Sanz, M. (2022). Valorization of alginate-extracted seaweed biomass for the development of cellulose-based packaging films. *Algal Research, 61*, Article 102576.
Ciuffarin, F., Négrier, M., Plazzotta, S., Libralato, M., Calligaris, S., Budtova, T., & Manzocco, L. (2023). Interactions of cellulose cryogels and aerogels with water and oil: Structure-function relationships. *Food Hydrocolloids, 140*, Article 108631.
De Eugenio, L. I., Escapa, I. F., Morales, V., Dinjaski, N., Galán, B., García, J. L., & Prieto, M. A. (2010). The turnover of medium-chain-length polyhydroxyalkanoates in Pseudomonas putida KT2442 and the fundamental role of PhaZ depolymerase for the metabolic balance. *Environmental Microbiology, 12*(1), 207–221.
de Oliveira, J. P., Bruni, G. P., El Halal, S. L. M., Bertoldi, F. C., Dias, A. R. G., & da Rosa Zavareze, E. (2019). Cellulose nanocrystals from rice and oat husks and their application in aerogels for food packaging. *International Journal of Biological Macromolecules, 124*, 175–184.
Díez, D., Urueña, A., Piñero, R., Barrio, A., & Tamminen, T. (2020). Determination of hemicellulose, cellulose, and lignin content in different types of biomasses by thermogravimetric analysis and pseudocomponent kinetic model (TGA-PKM method). *Processes, 8*(9), 1048.
Do, N. H., Luu, T. P., Thai, Q. B., Le, D. K., Chau, N. D. Q., Nguyen, S. T., … Duong, H. M. (2020). Heat and sound insulation applications of pineapple aerogels from pineapple waste. *Materials Chemistry and Physics, 242*, Article 122267.
Etale, A., Onyianta, A. J., Turner, S. R., & Eichhorn, S. J. (2023). Cellulose: A review of water interactions, applications in composites, and water treatment. *Chemical Reviews, 123*(5), 2016–2048.
Fabra, M. J., Pardo, P., Martínez-Sanz, M., Lopez-Rubio, A., & Lagarón, J. M. (2016). Combining polyhydroxyalkanoates with nanokeratin to develop novel biopackaging structures. *Journal of Applied Polymer Science, 133*(2).
Farooq, M., Sipponen, M. H., Seppälä, A., & Österberg, M. (2018). Eco-friendly flame-retardant cellulose nanofibril aerogels by incorporating sodium bicarbonate. *ACS Applied Materials & Interfaces, 10*(32), 27407–27415.
Feng, J., Nguyen, S. T., Fan, Z., & Duong, H. M. (2015). Advanced fabrication and oil absorption properties of super-hydrophobic recycled cellulose aerogels. *Chemical Engineering Journal, 270*, 168–175.
Fiol, N., Vásquez, M. G., Pereira, M., Tarrés, Q., Mutjé, P., & Delgado-Aguilar, M. (2019). TEMPO-oxidized cellulose nanofibers as potential Cu (II) adsorbent for wastewater treatment. *Cellulose, 26*, 903–916.
Freitas, P. A., González-Martínez, C., & Chiralt, A. (2022). Applying ultrasound-assisted processing to obtain cellulose fibres from rice straw to be used as reinforcing agents. *Innovative Food Science & Emerging Technologies, 76*, Article 102932.
García-González, C. A., Sosnik, A., Kalmár, J., De Marco, I., Erkey, C., Concheiro, A., & Alvarez-Lorenzo, C. (2021). Aerogels in drug delivery: From design to application. *Journal of Controlled Release, 332*, 40–63.
Hasan, M. A., Sangashetty, R., Esther, A. C. M., Patil, S. B., Sherikar, B. N., & Dey, A. (2017). Prospect of thermal insulation by silica aerogel: A brief review. *Journal of The Institution of Engineers (India): Series D, 98*, 297–304.
Hernández-Arriaga, A. M., Campano, C., Rivero-Buceta, V., & Prieto, M. A. (2022). When microbial biotechnology meets material engineering. *Microbial Biotechnology, 15*(1), 149–163.
Isogai, A., Saito, T., & Fukuzumi, H. (2011). TEMPO-oxidized cellulose nanofibers. *Nanoscale, 3*(1), 71–85.
Jiang, F., Han, S., & Hsieh, Y. L. (2013). Controlled defibrillation of rice straw cellulose and self-assembly of cellulose nanofibrils into highly crystalline fibrous materials. *RSC Advances, 3*(30), 12366–12375.
Jiang, S., Zhang, M., Li, M., Liu, L., Liu, L., & Yu, J. (2020). Cellulose nanofibril (CNF) based aerogels prepared by a facile process and the investigation of thermal insulation performance. *Cellulose, 27*, 6217–6233.
Kansiz, M., Domínguez-Vidal, A., McNaughton, D., & Lendl, B. (2007). Fourier-transform infrared (FTIR) spectroscopy for monitoring and determining the degree of crystallisation of polyhydroxyalkanoates (PHAs). *Analytical and Bioanalytical Chemistry, 388*, 1207–1213.

Kaur, A., & Kuhad, R. C. (2019). Valorization of rice straw for ethanol production and lignin recovery using combined acid-alkali pre-treatment. *BioEnergy Research, 12*, 570–582.

Kourmentza, C., Plácido, J., Venetsaneas, N., Burniol-Figols, A., Varrone, C., Gavala, H. N., & Reis, M. A. (2017). Recent advances and challenges towards sustainable polyhydroxyalkanoate (PHA) production. *Bioengineering, 4*(2), 55.

Le, W. T., Kankkunen, A., Rojas, O. J., & Yazdani, M. R. (2023). Leakage-free porous cellulose-based phase change cryogels for sound and thermal insulation. *Solar Energy Materials and Solar Cells, 256*, Article 112337.

Lindman, B., Karlström, G., & Stigsson, L. (2010). On the mechanism of dissolution of cellulose. *Journal of Molecular Liquids, 156*(1), 76–81.

Long, L. Y., Weng, Y. X., & Wang, Y. Z. (2018). Cellulose aerogels: Synthesis, applications, and prospects. *Polymers, 10*(6), 623.

Luo, R., Chen, J., Zhang, L., & Chen, G. (2006). Polyhydroxyalkanoate copolyesters produced by Ralstonia eutropha PHB− 4 harboring a low-substrate-specificity PHA synthase PhaC2Ps from Pseudomonas stutzeri 1317. *Biochemical Engineering Journal, 32*(3), 218–225.

Manoli, M. T., Blanco, F. G., Rivero-Buceta, V., Kniewel, R., Alarcon, S. H., Salgado, S., & Prieto, M. A. (2023). Heterologous constitutive production of short-chain-length polyhydroxyalkanoates in Pseudomonas putida KT2440: The involvement of IbpA inclusion body protein. *Frontiers in Bioengineering and Biotechnology, 11*.

Manoli, M. T., Nogales, J., & Prieto, A. (2022). Synthetic control of metabolic states in Pseudomonas putida by tuning polyhydroxyalkanoate cycle. *Mbio, 13*(1), Article e01794-21.

Martínez, V., de la Peña, F., García-Hidalgo, J., de la Mata, I., García, J. L., & Prieto, M. A. (2012). Identification and biochemical evidence of a medium-chain-length polyhydroxyalkanoate depolymerase in the Bdellovibrio bacteriovorus predatory hydrolytic arsenal. *Applied and Environmental Microbiology, 78*(17), 6017–6026.

Méndez, D. A., Schröter, B., Martínez-Abad, A., Fabra, M. J., Gurikov, P., & López-Rubio, A. (2023). Pectin-based aerogel particles for drug delivery: Effect of pectin composition on aerogel structure and release properties. *Carbohydrate Polymers, 306*, Article 120604.

Morcillo-Martín, R., Espinosa, E., Rabasco-Vílchez, L., Sanchez, L. M., de Haro, J., & Rodríguez, A. (2022). cellulose nanofiber-based aerogels from wheat straw: Influence of surface load and lignin content on their properties and dye removal capacity. *Biomolecules, 12*(2), 232.

Nair, S. S., Kuo, P. Y., Chen, H., & Yan, N. (2017). Investigating the effect of lignin on the mechanical, thermal, and barrier properties of cellulose nanofibril reinforced epoxy composite. *Industrial Crops and Products, 100*, 208–217.

Nayak, A. K., & Das, B. (2018). Introduction to polymeric gels. In *Polymeric gels* (pp. 3–27). Woodhead Publishing.

Panaitescu, D. M., Frone, A. N., & Chiulan, I. (2016). Nanostructured biocomposites from aliphatic polyesters and bacterial cellulose. *Industrial Crops and Products, 93*, 251–266.

Perera, K. Y., Jaiswal, A. K., & Jaiswal, S. (2023). Biopolymer-based sustainable food packaging materials: Challenges, solutions, and applications. *Foods, 12*(12), 2422.

Pérez-Bassart, Z., Fabra, M. J., Martínez-Abad, A., & López-Rubio, A. (2023). Compositional differences of β-glucan-rich extracts from three relevant mushrooms obtained through a sequential extraction protocol. *Food Chemistry, 402*, Article 134207.

Persano, F., Malitesta, C., & Mazzotta, E. (2024). Cellulose-based hydrogels for wastewater treatment: A focus on metal ions removal. *Polymers, 16*(9), 1292.

Pircher, N., Veigel, S., Aigner, N., Nedelec, J. M., Rosenau, T., & Liebner, F. (2014). Reinforcement of bacterial cellulose aerogels with biocompatible polymers. *Carbohydrate Polymers, 111*, 505–513.

Porras, M. A., Cubitto, M. A., & Villar, M. A. (2016). A new way of quantifying the production of poly (hydroxyalkanoate) s using FTIR. *Journal of Chemical Technology & Biotechnology, 91*(5), 1240–1249.

Reddy, V. U. N., Ramanaiah, S. V., Reddy, M. V., & Chang, Y. C. (2022). Review of the developments of bacterial medium-chain-length polyhydroxyalkanoates (mcl-PHAs). *Bioengineering, 9*(5), 225.

Reyes, A., Calleja, A., Gil-Guillén, I., & Benito-González, I. (2023). Optimization and characterization of reinforced biodegradable cellulose-based aerogels via polylactic acid/polyhydroxybutyrate coating. *International Journal of Biological Macromolecules, 253*, Article 127224.

Rivero-Buceta, V., Aguilar, M. R., Hernández-Arriaga, A. M., Blanco, F. G., Rojas, A., Tortajada, M., & Prieto, A. (2020). Anti-staphylococcal hydrogels based on bacterial cellulose and the antimicrobial biopolyester poly (3-hydroxy-acetylthioalkanoate-co-3-hydroxyalkanoate). *International Journal of Biological Macromolecules, 162*, 1869–1879.

Rodrigues, A. M., Franca, R. D. G., Dionísio, M., Sevrin, C., Grandfils, C., Reis, M. A., & Lourenço, N. D. (2022). Polyhydroxyalkanoates from a mixed microbial culture: Extraction optimization and polymer characterization. *Polymers, 14*(11), 2155.

Rodsamran, P., & Sothornvit, R. (2015). Renewable cellulose source: isolation and characterisation of cellulose from rice stubble residues. *International Journal of Food Science & Technology, 50*(9), 1953–1959.

Ross, G., Ross, S., & Tighe, B. J. (2017). Bioplastics: new routes, new products. *Brydson's Plastics Materials*, 631–652.

Sehaqui, H., Salajková, M., Zhou, Q., & Berglund, L. A. (2010). Mechanical performance tailoring of tough ultra-high porosity foams prepared from cellulose I nanofiber suspensions. *Soft Matter, 6*(8), 1824–1832.

Sescousse, R., Gavillon, R., & Budtova, T. (2011). Aerocellulose from cellulose–ionic liquid solutions: Preparation, properties and comparison with cellulose–NaOH and cellulose–NMMO routes. *Carbohydrate Polymers, 83*(4), 1766–1774.

Silva, J. B., Pereira, J. R., Marreiros, B. C., Reis, M. A., & Freitas, F. (2021). Microbial production of medium-chain length polyhydroxyalkanoates. *Process Biochemistry, 102*, 393–407.

Urbina, L., Eceiza, A., Gabilondo, N., Corcuera, M.Á., & Retegi, A. (2019). Valorization of apple waste for active packaging: Multicomponent polyhydroxyalkanoate coated nanopapers with improved hydrophobicity and antioxidant capacity. *Food Packaging and Shelf Life, 21*, Article 100356.

Wang, L., Borghei, M., Ishfaq, A., Lahtinen, P., Ago, M., Papageorgiou, A. C., … Rojas, O. J. (2020). Mesoporous carbon microfibers for electroactive materials derived from lignocellulose nanofibrils. *ACS sustainable chemistry & engineering, 8*(23), 8549–8561.

Wang, S., Chen, W., Xiang, H., Yang, J., Zhou, Z., & Zhu, M. (2016). Modification and potential application of short-chain-length polyhydroxyalkanoate (SCL-PHA). *Polymers, 8*(8), 273.

Wen, Y., Yuan, Z., Liu, X., Qu, J., Yang, S., Wang, A., … Ni, Y. (2019). Preparation and characterization of lignin-containing cellulose nanofibril from poplar high-yield pulp via TEMPO-mediated oxidation and homogenization. *ACS Sustainable Chemistry & Engineering, 7*(6), 6131–6139.

Xu, H., Sanchez-Salvador, J. L., Balea, A., Blanco, A., & Negro, C. (2022). Optimization of reagent consumption in TEMPO-mediated oxidation of Eucalyptus cellulose to obtain cellulose nanofibers. *Cellulose, 29*(12), 6611–6627.